The turbulent flow over a permeable wall

By W.P. Breugem † AND B.J. Boersma †

In this paper we discuss some turbulence statistics that are obtained from a Direct Numerical Simulation (DNS) of a turbulent flow in a channel of which one wall is permeable (porous, with zero net transpiration) and the other is impermeable. The flow within the porous wall is modeled using the Volume-Averaged Navier-Stokes equations (VANS). Among others, it is shown that wall permeability causes a considerable increase in the total drag, and an increased production of all Reynolds stresses when compared to an impermeable wall.

1. Introduction

There are many real-life cases of turbulent flows over porous media. Examples of this are flows over plant canopies, Finnigan (2000), and over river beds. In general it is assumed that these porous media increase the drag that the flow experiences, and enhance turbulent mixing near the wall. Not much is known about the physical mechanism that causes the drag increase.

In the present paper we study the flow over porous media in simple, two-dimensional geometries. First, we investigate the flow in a channel, which has one permeable and one impermeable wall. The second case is the spatially-developing boundary layer over a permeable wall. For the first case we will present statistics including the budgets in the transport equations for all Reynolds stresses. For the second case we will present only some preliminary results.

In the literature a porous medium is often represented simply by specifying boundary conditions at the wall, see e.g. Jiménez *et al.* (2001) and Hahn *et al.* (2002). In the paper of Jiménez *et al.* (2001), the wall-normal velocity component is assumed to be proportional to the wall-pressure fluctuation, whereas a no-slip condition is imposed for both the streamwise and the spanwise velocity components. In the paper of Hahn *et al.* (2002), the wall-normal velocity is assumed to be zero, and a slip velocity in both the streamwise and spanwise direction is imposed as given by the model of Beavers & Joseph (1967). In the present study we directly solve the governing equations for the flow within the porous medium together with the Navier-Stokes equations for the flow in the channel. The flow field is continuous over the interface between the porous medium and the channel, and hence no boundary conditions need to be prescribed at the interface. A fifth-order polynomial in the wall-normal coordinate is adopted to model the rapid variation of the porosity in a thin layer near the interface. Of course our approach results in a more complicated set of equations and larger computational costs than in the studies of Jiménez *et al.* (2001) and Hahn *et al.* (2002).

The organization of the paper is as follows. In section 2 we discuss the governing equations for the porous medium and give a short outline of the numerical method that

† Address: Laboratory for Aero and Hydrodynamics, J.M. Burgers Center, Leeghwaterstraat 21, 2628 CA Delft, The Netherlands.

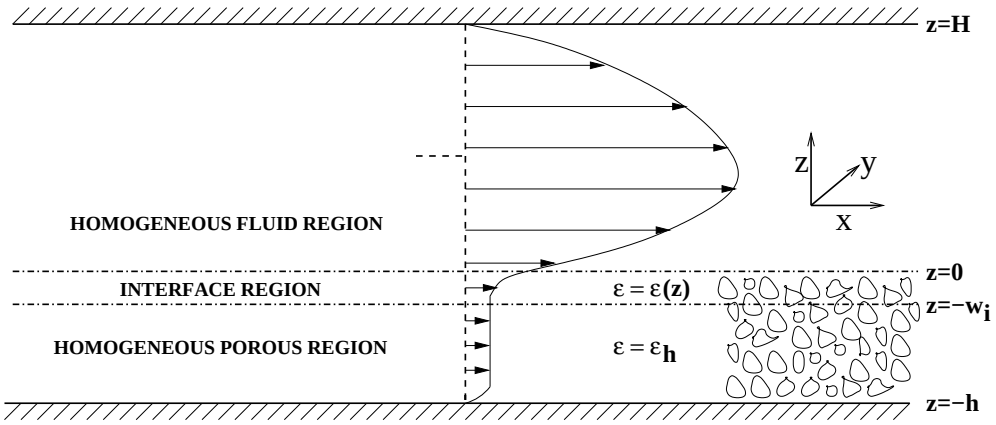

FIGURE 1. A sketch of the channel flow geometry (not on scale).

we use to solve these equations. In section 3 we present turbulence statistics obtained from a simulation such as mean-profiles, rms-profiles and Reynolds-stress budgets. Finally, in section 4 some conclusions are given.

2. Governing equations and numerical method

In this section we present the flow geometry, the governing equations for the flow along and through a porous medium, and the numerical method that we use to solve these equations.

2.1. *Governing equations*

In figure 1 we show the geometry of the channel flow. The flow is bounded by two impermeable walls located respectively on top of the two-dimensional channel (at $z = H$) and below the porous medium (at $z = -h$). Following Ochoa-Tapia & Whitaker (1995a), we distinguish between three regions:

(a) The homogeneous fluid region between $z = 0$ and $z = H$.

(b) The interface region between $z = -w_i$ and $z = 0$, which is characterized by rapid changes in the porous structure and the permeability.

(c) The homogeneous porous region between $z = -h$ and $z = -w_i$, with a constant porosity ($\epsilon = \epsilon_h$) and an isotropic permeability.

In the studies performed by Jiménez *et al.* (2001) and Hahn *et al.* (2002), the porous medium is modeled by specifying boundary conditions at the interface ($z = 0$). In contrast to their approaches, in our study we directly describe the flow inside the porous medium by means of the Volume-Averaged Navier-Stokes equations. These equations can be derived by averaging the standard Navier-Stokes equations for the flow inside the pores, over a small spatial volume. Figure 2 gives an illustration of the volume-averaging procedure. The constraints for the length scale R of the averaging volume are that it has to be much larger than the typical length scale l_β of the flow inside the pores, but also much smaller than the characteristic length scale of the volume-averaged flow.

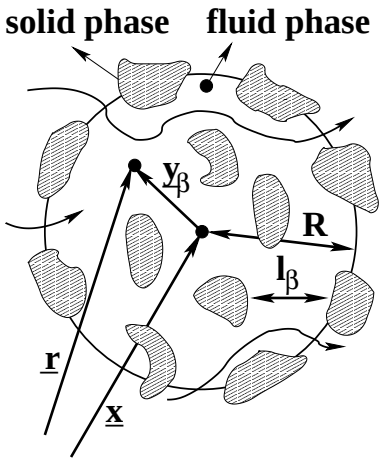

FIGURE 2. An illustration of the volume-averaging procedure.

It is important to distinguish between superficial and intrinsic volume-averages. The intrinsic velocity is denoted by square brackets and defined according to

$$<\underline{u}(\underline{x},t)>\equiv \frac{1}{V_\beta}\int_{V_\beta}\underline{u}(\underline{x}+\underline{y}_\beta,t)dV \tag{2.1}$$

where V_β is the part of the averaging volume V that is occupied by fluid. The vector $\underline{x}$ points to the centroid of the volume, and $\underline{y}_\beta$ is the position vector with respect to the centroid of V and points only into the fluid phase β (see figure 2). The subscript β refers to the fluid or β–phase, in distinction to the solid or σ–phase. The superficial velocity is related to the intrinsic velocity according to

$$<\underline{u}(\underline{x},t)>^s\equiv \frac{1}{V}\int_{V_\beta}\underline{u}(\underline{x}+\underline{y}_\beta,t)dV=\epsilon<\underline{u}(\underline{x},t)> \tag{2.2}$$

where the superscript s refers to the superficial instead of the intrinsic average. The porosity ϵ is the ratio of the volume taken up by the fluid phase to the total averaging volume, i.e.

$$\epsilon\equiv\frac{V_\beta}{V}$$

Notice that the superficial and intrinsic averages are defined everywhere inside the porous medium, in the β-phase as well as in the σ-phase.

The local deviations of the velocity and pressure insides the pores from the corresponding volume-averaged quantities are denoted by a tilde and defined as respectively

$$\underline{\tilde{u}}\equiv\underline{u}-<\underline{u}>$$

$$\tilde{p}\equiv p-<p>$$

By applying the volume-averaging procedure to the Navier-Stokes equations for the incompressible flow inside the pores, Whitaker (1996) gives a formal derivation of the Volume-Averaged Navier-Stokes equations. The result reads:

$$\frac{D<\underline{u}>}{Dt}+\epsilon^{-1}\nabla\cdot<\underline{\tilde{u}\tilde{u}}>^s=-\frac{1}{\rho}\nabla<p>+\nu\nabla^2<\underline{u}>+$$

$$\nu\frac{\nabla\epsilon}{\epsilon}\nabla<\underline{u}>+\nu\frac{\nabla^2\epsilon}{\epsilon}<\underline{u}>+$$
$$\frac{1}{\rho}\frac{1}{V_\beta}\int_{A_{\beta\sigma}}\underline{n}_{\beta\sigma}\cdot(-\underline{\underline{I}}\tilde{p}+\mu\nabla\underline{\tilde{u}})dA \tag{2.3}$$

$$\nabla\cdot(\epsilon<\underline{u}>)=0 \tag{2.4}$$

where $A_{\beta\sigma}$ is the contact area between the β– and σ–phase within the averaging volume, $\underline{n}_{\beta\sigma}$ the normal vector pointing into the σ–phase, and $\underline{\underline{I}}$ the unity tensor. For homogeneous porous media (ϵ = constant) the terms containing derivatives of the porosity are zero, and so these terms are significant only in the interface region (see figure 1). Notice from equation (2.4) that when the porosity is varying in space, only the superficial and not the intrinsic velocity is divergence-free.

We need closures for the second term at the left-hand-side and the last term at the right-hand-side of equation (2.3). The second term on the left-hand-side of equation (2.3) is a dispersive flux term. It represents the effect of spatial correlations between flow variations inside the pores, on the volume-averaged flow. In the literature it is often implicitly assumed that this term can be neglected, as we will do in the present study. For the last term on the right-hand-side of equation (2.3), Whitaker (1996) formulates a closure problem in which the surface integral is replaced by the following expression

$$\frac{1}{\rho}\frac{1}{V_\beta}\int_{A_{\beta\sigma}}\underline{n}_{\beta\sigma}\cdot(-\underline{\underline{I}}\tilde{p}+\nu\nabla\underline{\tilde{u}})dA=-\nu\epsilon\underline{\underline{K}}^{-1}\cdot<\underline{u}>^\beta-\nu\epsilon(\underline{\underline{K}}^{-1}\cdot\underline{\underline{F}})\cdot<\underline{u}>^\beta \tag{2.5}$$

where $\underline{\underline{K}}$ and $\underline{\underline{F}}$ are referred to as respectively the (yet unknown) permeability and the Forchheimer tensor. The first term on the right-hand side of equation (2.5) is known as the Darcy term, and it basically represents the effect of the viscous drag that the flow inside the pores encounters. The second term on the right-hand side represents the effect of pressure drag on the flow inside the pores. In the literature semi–empirical relationships are available for the tensors $\underline{\underline{K}}$ and $\underline{\underline{F}}$ for homogeneous porous media. Based on one of these relations, known as the Ergun equation - see MacDonald *et al.* (1979) - the Forchheimer and permeability parameters can then be expressed by the following scalars

$$F=\frac{1}{100(1-\epsilon)}\frac{d_p\|<\underline{u}>^s\|}{\nu} \tag{2.6}$$

$$K=\frac{{d_p}^2\epsilon^3}{180(1-\epsilon)^2} \tag{2.7}$$

with the mean particle diameter d_p defined as six times the ratio of the total volume V_p to the total surface area A_p of the σ–phase

$$d_p\equiv\frac{6V_p}{A_p} \tag{2.8}$$

The major advantage of a direct description of the flow inside the porous medium is that we do not need to prescribe any boundary conditions at the interface, because the flow field is continuous over the interface. Yet we have to deal with another problem as strictly speaking the closure (2.5) is not valid in the interface region. The thickness of the interface region is on the order of the mean particle diameter, and inside this region the flow field is very complicated due to roughness. In our present study we use a variable-porosity-model for the interface region, see Ochoa-Tapia & Whitaker (1995b), and still assume the validity of the closure in this region. The porosity is described by a fifth-order

polynomial in the wall-normal coordinate, such that it satisfies the requirements that its derivatives are zero at $z = 0$ and $z = -w_i$, that at $z = 0$ the porosity equals 1, and that at $z = -w_i$ its value is equal to ϵ_h.

2.2. *Numerical method*

The governing equations (2.3) and (2.4) are discretized with a pseudo-spectral method in the x- and y-directions and with a second-order finite-difference method in the direction perpendicular to the porous medium, i.e. the z-direction. The (staggered) grid in this direction is non-uniform with points clustered around the interface ($z = 0$) between the clear fluid and the porous medium. The solution is advanced in time with a second-order explicit Adams-Bashforth method. The pressure-correction method is used to ensure conservation of mass. The flow in both the porous medium and the channel is forced in the x-direction by a constant pressure gradient dp/dx.

3. Results

In this section we present some turbulence statistics that are obtained from a fully developed channel flow simulation over a permeable wall. The simulation is one of the first that we performed to test our DNS code. The porosity in the homogeneous porous region is high and equal to $\epsilon_h = 0.95$. In table 1 some characteristics of the simulation are listed. As the flow in the channel is asymmetric, the Reynolds number based on the friction velocity at the upper wall is different from the corresponding Reynolds number based on the square root of the total stress at the interface with the lower wall. The Reynolds number based on the bulk velocity in the channel is 4517. The thickness of the porous medium is 1/16 of the channel height. In this simulation the thickness of the interface region is set equal to the thickness of the porous medium as this requires less grid points in the porous medium. The numerical resolution of this test-simulation is coarse with grid spacings in (upper) wall-units of $dx^+ = 33.9$, $dy^+ = 20.3$, $dz^+_{min} = 1.0$ and $dz^+_{max} = 5.1$ for the streamwise, spanwise and wall-normal directions, respectively. The stretch factor for the grid spacing in the wall-normal direction is 2.5 % for both the porous medium and the channel. Unfortunately, there is a jump in the grid spacing over the interface where the first grid cell above the interface is a factor 2.2 smaller than the first grid cell below the interface. The simulation is run until the bulk velocity reached a steady state. Once the flow reached a steady state, 60 data fields were stored each equally separated in time by H/u_*, with u_* the friction velocity at the upper wall. The statistics in this study are obtained from these 60 data fields. The simulation has been performed on a AMD-Athlon with 1Gb of core memory.

To start with we show the mean-velocity profile. (figure 3). The dashed line marks the interface with the permeable wall. Clearly, there is a non-zero velocity (slip-velocity) at the interface. The velocity profile has its maximum above the centerline of the channel, already indicating a higher total shear stress at the permeable wall.

In figure 4 we show the root-mean-square profiles of the three velocity components and of the pressure, normalized with the friction velocity at the upper wall. Near the upper wall, the rms-profiles behave as expected and are similar to the profiles for standard channel flow. The rms-profiles near the lower wall are clearly altered by wall permeability. A strong increase can be observed in the spanwise and wall-normal velocity fluctuations, and in the pressure fluctuations. The axial rms has its peak just at the interface, with a value slightly smaller than at the peak near the upper impermeable wall.

In figure 5 the turbulent and viscous stresses as a function of the channel height are

$Re_*(top)$	325.
$Re_*(bottom)$	393.
Re_b	4517.
$N_x \times N_y \times N_z$	$48 \times 48 \times (128 + 8)$
$L_x \times L_y \times L_z$	$5 \times 3 \times (1 + 1/16)$
ϵ_h	0.95
d_p	1/125
w_i	1/16

TABLE 1. Characteristics of the channel flow simulation.

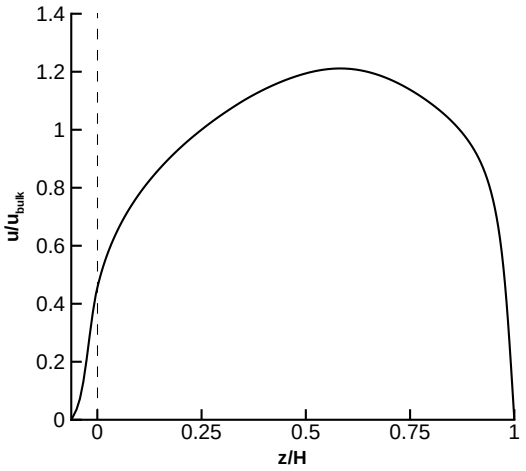

FIGURE 3. The mean velocity profile as function of the channel height. The dashed line marks the position of the interface between the porous medium and the clear fluid.

plotted. The total stress (sum of the viscous plus the turbulent stress) is linear, which is a direct consequence of the constant pressure gradient that drives the flow. We clearly observe a strong increase in drag on the lower permeable wall compared to the upper solid wall. In this simulation the drag increase is almost 50 %. This increase in drag is caused by the exchange of momentum between the clear fluid and the porous medium. In engineering appliances porous materials are sometimes used as heat-exchanger. From the results presented in figures 4 and 5, it is clear that a porous wall aligned parallel to the mean-flow direction will indeed give a very efficient turbulent heat exchange between the flow over and the flow in the porous medium (the behavior of the turbulent heat flux $\overline{<u'><T'>}$ will be very similar to that of the turbulent stress $\overline{<u'><w'>}$).

To get a better insight into the mechanisms behind the drag increase we have calculated the budgets of the transport equations of all the individual Reynolds stresses. The terms are made dimensionless with u_*^4/ν, where u_* is the friction velocity at the upper wall. The exact equations are given in Appendix A. In figure 6 the budgets of the transport equation for the streamwise normal stress (streamwise contribution to turbulent kinetic

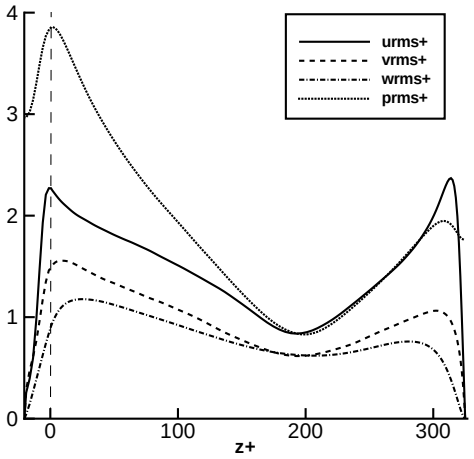

FIGURE 4. The rms-profiles of the streamwise, spanwise and wall-normal velocity fluctuations together with the rms-profile of the pressure, all normalized by friction velocity.

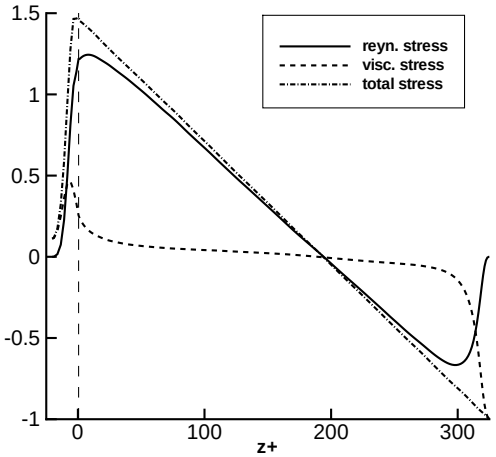

FIGURE 5. The turbulent, viscous and total stress profiles as a function of the channel height.

energy) are shown. The left part of the figure gives the budgets near the permeable wall and the right part the budgets near the upper impermeable wall. The budgets in the upper part of the channel are similar to the budgets calculated by Mansour *et al.* (1988) for standard channel flow between two impermeable walls. Very close to the upper wall the dissipation term (uuDISS) is balanced by the transport term (uuTRANS). At more than about 40 wall units from the upper wall, the pressure-strain term (uuPS) is on the order of the dissipation term and their sum balances the production term (uuPROD). At the lower permeable wall the budgets have changed dramatically. Just above the interface the production term is balanced by the sum of the transport term, the pressure-strain term and the dissipation term. Within the porous wall, the Forchheimer

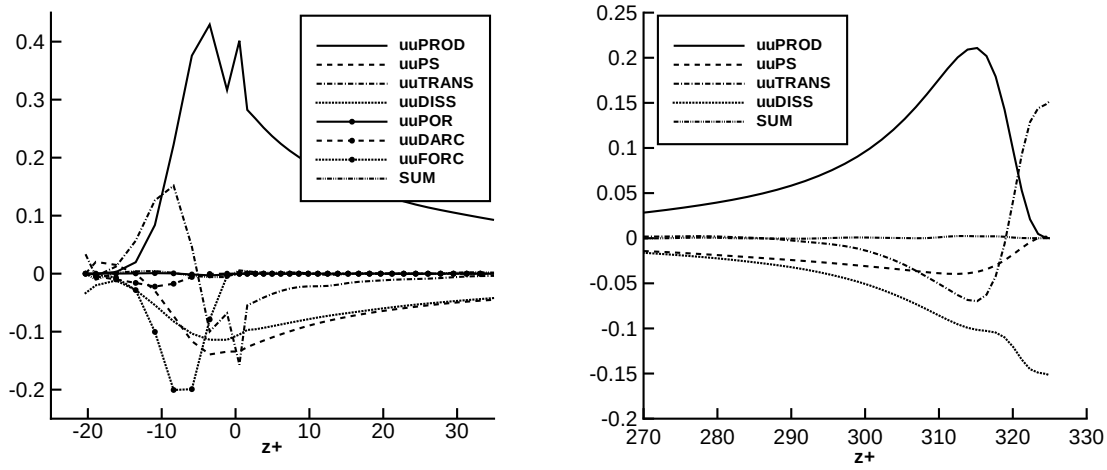

FIGURE 6. The budget of the transport equation for the streamwise contribution to turbulent kinetic energy. Left: the budget at the lower permeable wall (the interface is located at $z = 0$). Right: the budget at the upper wall. (The 'kink' in the production term (uuPROD) and in the transport term (uuTRANS) is a consequence of the jump in the wall-normal grid spacing over the interface, as mentioned before at the beginning of this section.)

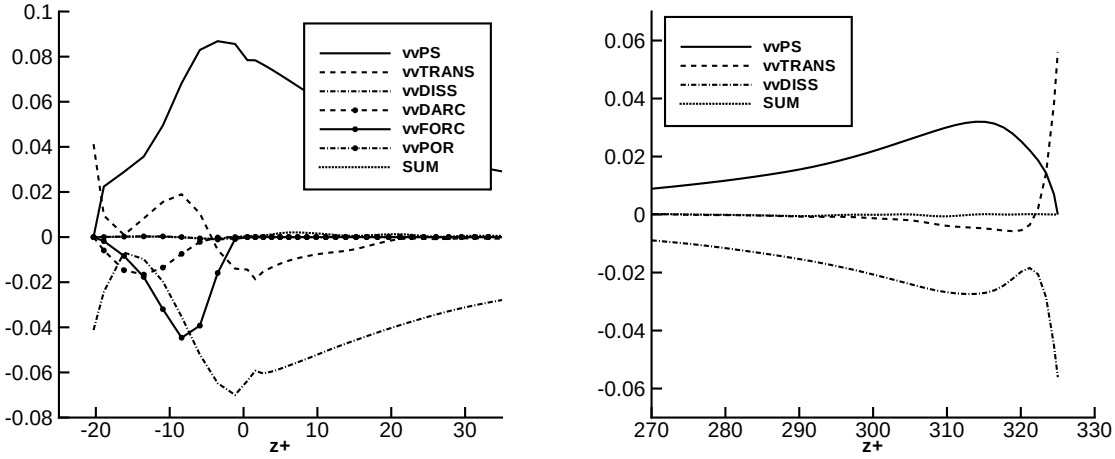

FIGURE 7. The budget of the transport equation for the spanwise contribution to turbulent kinetic energy. Left: The budget at the lower permeable wall (the interface is located at $z = 0$). Right: The budget at the upper wall.

term (uuFORC) becomes the dominant loss term, but it vanishes again close to the impermeable wall below the porous medium. The Darcy term (uuDARC) is of minor importance, a consequence of the high porosity of the wall. The porosity term (uuPOR) basically represents the sum of the advection and the production/dissipation of kinetic energy by changes in the porous structure. It appears to be negligible in this simulation,

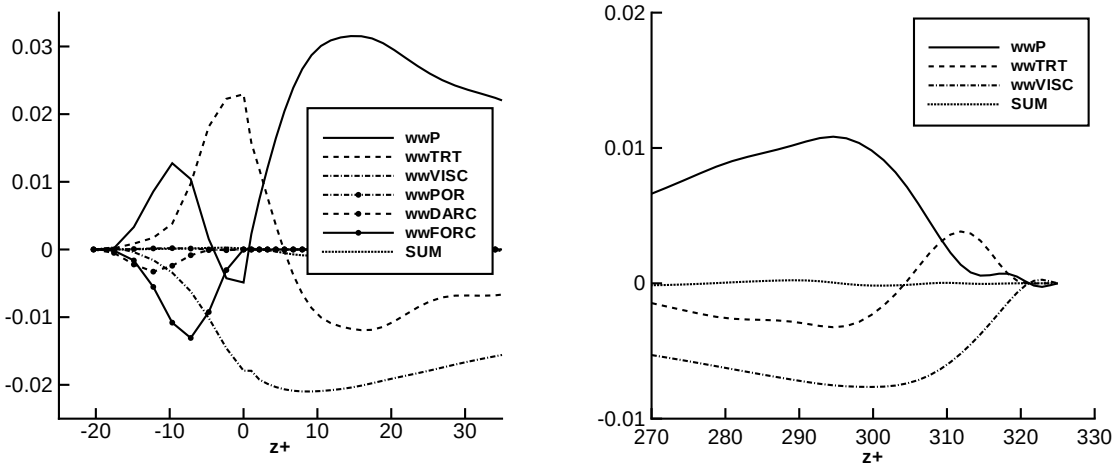

FIGURE 8. The budget of the transport equation for the wall-normal contribution to turbulent kinetic energy. Left: The budgets at the lower permeable wall (the interface is located at $z = 0$). Right: The budgets at the upper wall.

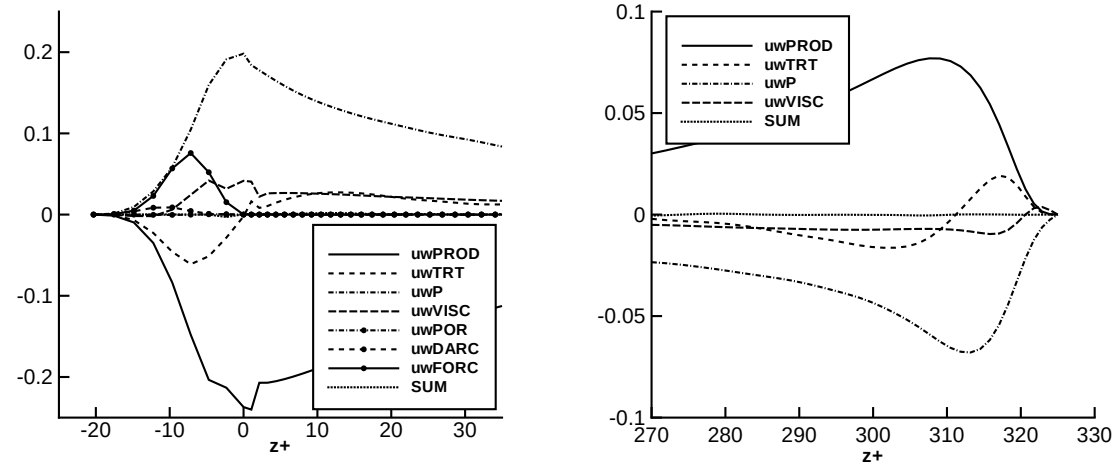

FIGURE 9. The budget of the transport equation for the Reynolds stress $\overline{<u'><w'>}$. Left: the budgets at the lower permeable wall (the interface is located at $z = 0$). Right: the budgets at the upper wall.

because of the high porosity and the large width of the interface region over which the porosity is varying. Notice also from figure 6 that the peak in the production term just below the permeable interface is roughly twice as large as the corresponding peak near the upper wall.

In figure 7 the budgets of the transport equation for the spanwise kinetic energy are shown. Again the left graph shows the budgets near the permeable wall, and the right graph the budgets near the upper wall. At the upper wall the pressure-strain term (vvPS)

balances the dissipation term (vvDISS), except in a region less than about 5 wall units from the wall. In this small region the pressure-strain term falls off to zero and the transport of energy (vvTRANS) by viscous diffusion balances the dissipation. Above the interface with the lower permeable wall, the transport term remains small and there is basically a balance between only the pressure-strain term and the dissipation term. Inside the porous wall, the Forchheimer term becomes the dominant loss term in a small region. The porosity term (vvPOR) is not significant, and the Darcy term (vvDARC) is only of importance in a region of roughly 10 wall units close to the impermeable wall below the porous medium. As we saw before for the production term in the axial case, in the spanwise case the pressure-strain term has a peak inside the porous medium which is more than twice as large as the corresponding peak near the upper wall. The pressure-strain term is a redistribution term, which is responsible for the transfer of axial kinetic energy into spanwise and wall-normal kinetic energies. The enormous increase in this term near the permeable wall explains the increase in the rms of the spanwise velocity fluctuations near the permeable wall as compared to the peak at the upper wall.

In figure 8 the budgets in the transport equation for the wall-normal kinetic energy are shown. Close to the upper wall, the velocity-pressure-gradient term (wwP) becomes smaller than the turbulent-transport term (wwTRT). This behavior is slightly different from that of a standard channel flow described by Mansour *et al.* (1988), where close to the wall the turbulent-transport term is still smaller than the velocity-pressure-gradient term. The reason for this discrepancy might be a matter of grid resolution, as we have in our simulation a coarse grid. In the region just above the interface with the permeable wall, the turbulent-transport term changes of sign and is responsible for a flux of wall-normal kinetic energy into the porous medium. Strangely enough, the velocity-pressure-gradient term is negative in a small region around the interface. In this region the only source of wall-normal kinetic energy comes from the turbulent-transport term. Inside the porous medium there is again a region where the Forchheimer term (wwFORC) is the most important loss term. The Darcyterm (wwDARC) is of minor importance except close to the impermeable wall below the porous medium. The porosity term (wwPOR) is everywhere negligible. Notice that the velocity-pressure-gradientterm has a peak above the permeable interface, which is almost three times larger than the corresponding peak near the upper wall. This energy-redistribution term is responsible for the increase in the rms of the wall-normal velocity fluctuations near the permeable wall as compared to the peak at the upper wall.

In figure 9 the budgets of the transport equation for the turbulent stress ($\overline{<u'><w'>}$) are shown. At the upper as well as near the lower permeable wall, the leading terms are the production term (uwPROD) and the velocity-pressure-gradient term (uwP). Different from the case for the kinetic energies, the Forchheimer term is nowhere the leading loss term. The Darcy term (uwDARC) and the porosity term (uwPOR) are negligible. It is striking that near the permeable interface, the peak values of the production termg and the velocity-pressure-gradient term are more than twice as large as the corresponding peak values near the upper wall. The increase in the production term is caused solely by the enormous increase in the wall-normal velocity fluctuations as the gradient of the mean velocity near the permeable interface is reduced as compared to the upper wall.

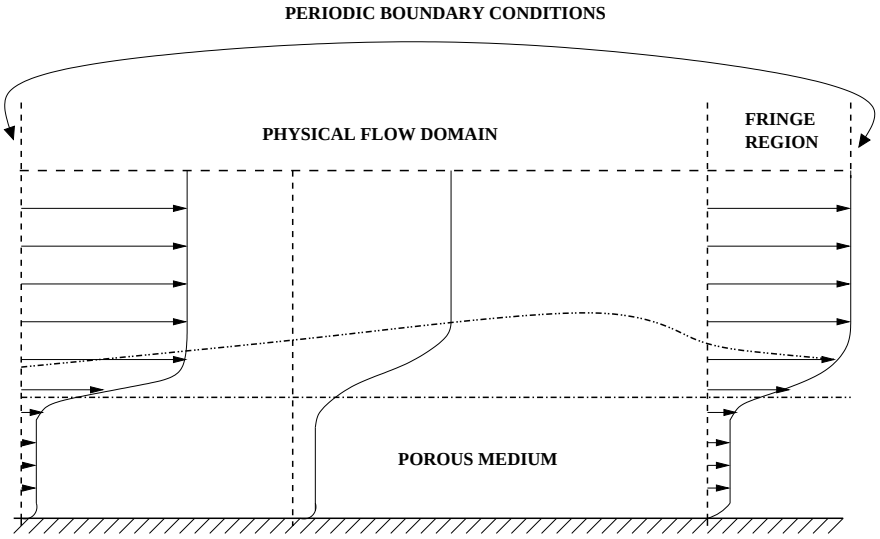

FIGURE 10. A sketch of the computational domain for the simulation of the spatially developing boundary layer over a permeable wall.

4. The turbulent boundary layer over a permeable wall.

In the previous section we presented some results for the flow over a porous channel wall. It was assumed that the flow in the channel was fully developed. In this section we will give some preliminary results for a turbulent, spatially-developing boundary layer over a permeable wall.

The boundary layer is not periodic in the streamwise direction. However, we would like to use the pseudo-spectral method as outlined in the previous section. This method requires that the flow field can be considered as periodic in the streamwise direction. In order to make the problem periodic we have added a 'fringe' region to our domain in which an artificial force drives the velocity field to a specified target. This is illustrated in figure 10. This fringe region can also be seen as a region in which the mean flow in the boundary layer is accelerated and where turbulent kinetic energy is dissipated. A first result of these simulations is shown in figure 11. The porosity in the homogeneous porous region is 0.8. The thickness w_i of the interface region is equal to $1/25\ H$, where H is the height of the flow domain above the permeable interface. The thickness of the porous medium is $0.4\ H$. The mean particle diameter associated with the porous medium is $1/62.5\ H$. The dimensions of the flow domain are $L_x \times L_y \times L_z = 20 \times 3 \times (1 + 0.4)$ for respectively the streamwise, spanwise and wall-normal direction. The artificial force in the fringe region is a smooth function of the streamwise coordinate and has a significant value over a length of about $2\ H$. The number of grid points is $192 \times 64 \times (82 + 24)$ for respectively the streamwise, spanwise and wall-normal direction.

5. Conclusions

In this paper we have presented results from a direct numerical simulation of the flow over and through a permeable wall forming one wall of a channel with fully-developed turbuloent flow. In contrast to the simulations presented in the literature, Jiménez *et al.* (2001) and Hahn *et al.* (2002), we have solved for the flow in the channel coupled with

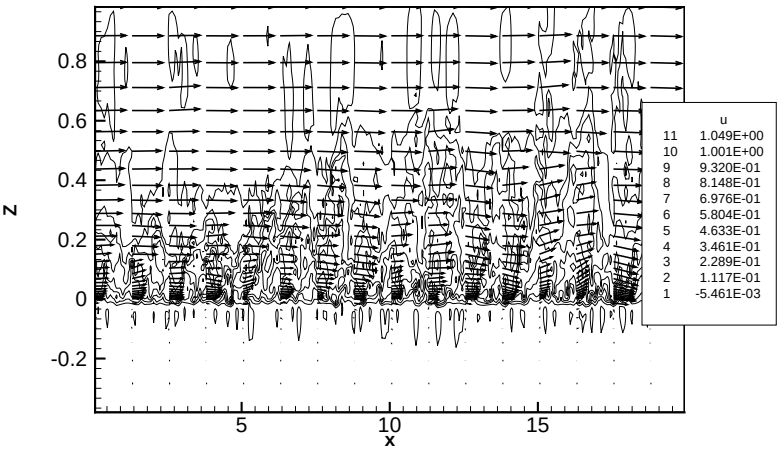

FIGURE 11. A preliminary result of a simulation of the spatially developing boundary layer over a permeable wall. The graph shows an instantaneous snapshot of the velocity field (u, w) in plane with y=constant, where the solid lines are contours of constant streamwise velocity.

the flow in the porous medium. Over the interface with the permeable wall, the flow is continuous and hence no boundary conditions need to be prescribed at the interface. From the simulation we observe a considerable increase in the total drag at the permeable wall. This is caused by the exchange of wall-normal momentum through the interface with the wall, resulting in a higher Reynolds stress $\overline{<u'><w'>}$ as compared to the impermeable wall. The budgets in the transport equations for all the Reynolds stresses have demonstrated that for the evaluated simulation with a porosity of 0.95, the Darcy term is small compared to the Forchheimer term. The Darcy term represents the loss of Reynolds stresses by the viscous drag that the flow inside the pores encounters. The Forchheimer term represents losses due to the pressure drag acting on the flow inside the pores. The porosity term, which represents the advection and production/dissipation of Reynolds stresses by porosity variations, appears to be negligible throughout the porous medium. Furthermore, a start has been made with the simulation of a spatially developing boundary layer over a permeable wall.

Appendix A. transport equations for all the Reynolds stresses

In the following equations, the velocity components and the pressure are all intrinsic volume-averages, but for clarity we have omitted the square brackets.

- transport equation for the axial kinetic energy $\frac{1}{2}\overline{u'^2}$.

$$0 = \underbrace{-\overline{u'w'}\frac{\partial \overline{u}}{\partial z}}_{uuPROD} + \underbrace{\overline{p'\frac{\partial u'}{\partial x}}}_{uuPS} + \underbrace{\frac{\partial}{\partial z}\left(\frac{1}{Re}\frac{1}{2}\frac{\partial \overline{u'^2}}{\partial z}\right) - \frac{1}{\epsilon}\frac{\partial}{\partial z}\left(\epsilon\frac{1}{2}\overline{u'^2 w'}\right)}_{uuTRANS}$$

$$
\begin{aligned}
&\underbrace{-\frac{1}{Re}\overline{\left(\frac{\partial u'}{\partial x}\right)^2+\left(\frac{\partial u'}{\partial y}\right)^2+\left(\frac{\partial u'}{\partial z}\right)^2}}_{uuDISS}\\
&\underbrace{+\frac{1}{2}\frac{1}{Re}\frac{1}{\epsilon}\frac{\partial\epsilon}{\partial z}\frac{\partial\overline{u'^2}}{\partial z}+\frac{1}{Re}\frac{1}{\epsilon}\frac{\partial^2\epsilon}{\partial z^2}\overline{u'^2}}_{uuPOR}-\underbrace{\frac{1}{Re}\frac{\epsilon}{Da}\overline{u'^2}}_{uuDARC}-\underbrace{\frac{1}{Re}\frac{\epsilon}{Da}\overline{u'\left[F\cdot u-\overline{F\cdot u}\right]}}_{uuFORC}
\end{aligned}
$$

- transport equation for the spanwise kinetic energy $\frac{1}{2}\overline{v'^2}$.

$$
\begin{aligned}
0=&\underbrace{\overline{p'\frac{\partial v'}{\partial x}}}_{vvPS}+\underbrace{\frac{\partial}{\partial z}\left(\frac{1}{Re}\frac{1}{2}\frac{\partial\overline{v'^2}}{\partial z}\right)-\frac{1}{\epsilon}\frac{\partial}{\partial z}\left(\epsilon\frac{1}{2}\overline{v'^2w'}\right)}_{vvTRANS}\\
&\underbrace{-\frac{1}{Re}\overline{\left(\frac{\partial v'}{\partial x}\right)^2+\left(\frac{\partial v'}{\partial y}\right)^2+\left(\frac{\partial v'}{\partial z}\right)^2}}_{vvDISS}\\
&\underbrace{+\frac{1}{2}\frac{1}{Re}\frac{1}{\epsilon}\frac{\partial\epsilon}{\partial z}\frac{\partial\overline{v'^2}}{\partial z}+\frac{1}{Re}\frac{1}{\epsilon}\frac{\partial^2\epsilon}{\partial z^2}\overline{v'^2}}_{vvPOR}-\underbrace{\frac{1}{Re}\frac{\epsilon}{Da}\overline{v'^2}}_{vvDARC}-\underbrace{\frac{1}{Re}\frac{\epsilon}{Da}\overline{v'\left[F\cdot v-\overline{F\cdot v}\right]}}_{vvFORC}
\end{aligned}
$$

- transport equation for the wall-normal kinetic energy $\frac{1}{2}\overline{w'^2}$.

$$
\begin{aligned}
0=&\underbrace{\overline{p'\frac{\partial w'}{\partial z}}-\frac{\partial}{\partial z}\overline{p'w'}}_{wwP}-\underbrace{\frac{1}{\epsilon}\frac{\partial}{\partial z}\left(\epsilon\frac{1}{2}\overline{w'^2w'}\right)}_{wwTRT}\\
&\underbrace{+\frac{\partial}{\partial z}\left(\frac{1}{Re}\frac{1}{2}\frac{\partial\overline{w'^2}}{\partial z}\right)-\frac{1}{Re}\overline{\left(\frac{\partial w'}{\partial x}\right)^2+\left(\frac{\partial w'}{\partial y}\right)^2+\left(\frac{\partial w'}{\partial z}\right)^2}}_{wwVISC}\\
&\underbrace{+\frac{1}{2}\frac{1}{Re}\frac{1}{\epsilon}\frac{\partial\epsilon}{\partial z}\frac{\partial\overline{w'^2}}{\partial z}+\frac{1}{Re}\frac{1}{\epsilon}\frac{\partial^2\epsilon}{\partial z^2}\overline{w'^2}}_{wwPOR}-\underbrace{\frac{1}{Re}\frac{\epsilon}{Da}\overline{w'^2}}_{wwDARC}-\underbrace{\frac{1}{Re}\frac{\epsilon}{Da}\overline{w'\left[F\cdot w'-\overline{F\cdot w'}\right]}}_{wwFORC}
\end{aligned}
$$

- Tranport equation for the turbulent stress $\overline{u'w'}$.

$$
\begin{aligned}
0=&\underbrace{-\overline{w'^2}\frac{\partial\overline{u}}{\partial z}}_{uwPROD}\underbrace{-\frac{1}{\epsilon}\frac{\partial}{\partial z}\left(\epsilon\overline{w'^2u'}\right)}_{uwTRT}\underbrace{+\overline{p'\left(\frac{\partial u'}{\partial z}+\frac{\partial w'}{\partial x}\right)}-\frac{\partial\overline{p'u'}}{\partial z}}_{uwP}\\
&\underbrace{-\frac{2}{Re}\overline{\left(\frac{\partial u'}{\partial x}\frac{\partial w'}{\partial x}\right)+\left(\frac{\partial u'}{\partial y}\frac{\partial w'}{\partial y}\right)+\left(\frac{\partial u'}{\partial z}\frac{\partial w'}{\partial z}\right)}+\frac{1}{R}\frac{\partial^2\overline{u'w'}}{\partial z^2}}_{uwVISC}\\
&\underbrace{+\frac{1}{Re}\frac{1}{\epsilon}\frac{\partial\epsilon}{\partial z}\frac{\partial\overline{u'w'}}{\partial z}+\frac{2}{Re}\frac{1}{\epsilon}\frac{\partial^2\epsilon}{\partial z^2}\overline{u'w'}}_{uwPOR}-\underbrace{\frac{1}{Re}\frac{\epsilon}{Da}\overline{u'w'}}_{uwDARC}
\end{aligned}
$$

$$\underbrace{-\frac{1}{Re}\frac{\epsilon}{Da}\overline{w'\left[F\cdot u-\overline{F\cdot u}\right]}-\frac{1}{Re}\frac{\epsilon}{Da}\overline{u'\left[F\cdot w'-\overline{F\cdot w'}\right]}}_{uwFORC}$$

REFERENCES

MacDonald, I.F., El-Sayed, M.S., Mow, K. & Dullien, F.A.L. 1979 Flow through porous media: The Ergun equation revisited. *Ind. and Eng. Chemistry* **18**, 199-208.

Whitaker, S. 1996 The Forchheimer equation: a theoretical development. *Transport in Porous Media* **25**, 27-61.

Finnigan, J. 2000 Turbulence in plant canopies. *Annu. Review Fluid Mech.* **32** 519-571.

Beavers, G.S., & Joseph, D.D. 1967 Boundary conditions at a naturally permeable wall. *J. Fluid Mech.* **30**, 197-207.

Mansour, N.N., Kim,J. & Moin, P. 1988 Reynolds-stress and dissipation-rate budgets in a turbulent channel flow. *J. Fluid Mech.* **194**. 15-44.

Hahn, S., Je, J. & Choi, H. 2002 Direct numerical simulation of turbulent channel flow with permeable walls. *J. Fluid Mech.* **450**, 259-285.

Jiménez, J., Uhlmann, M., Pinelli, A. & Kawahara, G. 2001 Turbulent shear flow over active and passive porous surfaces. *J. Fluid Mech.* **442**, 89-117.

Spalart, P.R. 1988 Direct simulation of a turbulent boundary layer up to $Re_\theta = 1410$. *J. Fluid Mech.* **187**, 61-98.

Ochoa-Tapia, J.A. & Whitaker, S. 1995a Momentum transfer at the boundary between a porous medium and a homogeneous fluid – I. Theoretical development. *Int. J. Heat Mass Transfer* **38**, 2635-2646.

Ochoa-Tapia, J.A. & Whitaker, S. 1995b Momentum transfer at the boundary between a porous medium and a homogeneous fluid – II. Comparison with experiment. *Int. J. Heat Mass Transfer* **38**, 2647-2655.